Quantum Efficiency Measurement

Of Nanowires Using Integrating Sphere

by

Dongzi Chen

A Thesis Presented in Partial Fulfillment
of the Requirement for the Degree
Master of Science

Approved April 2012 by the
Graduate Supervisory Committee:

Cun-Zheng Ning, Chair
Yong-Hang Zhang
Hongbin Yu

ARIZONA STATE UNIVERSITY

May 2012

ABSTRACT

This thesis mainly focuses on the study of quantum efficiency (QE) and its measurement, especially for nanowires (NWs). First, a brief introduction of nano-technology and nanowire is given to describe my initial research interest. Next various fundamental kinds of recombination mechanisms are described; both for radiative and non-radiative processes. This is an introduction for defining the internal quantum efficiency (IQE). A relative IQE measurement method is shown following that.

Then it comes to the major part of the thesis discussing a procedure of quantum efficiency measurement using photoluminescence (PL) method and an integrating sphere, which has not been much applied to nanowires (NWs). In fact this is a convenient and useful approach for evaluating the quality of NWs since it considers not only the PL emission but also the absorption of NWs. The process is well illustrated and performed with both wavelength-dependent and power-dependent measurements. The measured PLQE is in the range of 0.3% ~ 5.4%. During the measurement, a phenomenon called photodegradation is observed and examined by a set of power-dependence measurements. This effect can be a factor for underestimating the PLQE and a procedure is introduced during the sample preparation process which managed to reduce this effect for some degree.

TABLE OF CONTENTS

Page

CHAPTER Page

LIST OF FIGURES

Figure Page

Figure Page

1. Introduction:

1.1 Nanotechnology and Nanowire

Nanotechnology, which focuses on the controlling object on an atomic and molecular scale, is a vastly developed research area these years. Actually its fundamental concepts are developed much earlier. During 1980s, more and more investigations have been looked into it, especially after the experimental advances in microscopy, such as the invention of scanning tunneling microscope in 1981[1], which can take surface image at the atomic level. Among the diverse concepts of nanotechnology, nanowire (NW) is a prospective area within nanostructure materials, which has a two-dimensional (thickness and width/diameter) confinement of the order of 10^{-8} ~ 10^{-9} meter while free of constraint along the length direction.

Semiconductor NWs, among the many different types of NWs, is a particularly attractive interest due to their distinct characteristics with semiconductors. The bandgap, carrier density, donor and acceptor impurities are all possible factors to be manipulated for specific application. Not to mention the semiconductors can perform very differently under distinct temperature, pressure, or external effect such as electrical injection or optical excitation. The bandgap engineering, which will be mentioned later, is such a good example. By setting different alloy composition during synthesizing, the

bandgap of semiconductor NWs, which deciding the wavelength of emitted photons, can be tailored for covering a broad range of spectrum.

From another point of view, the semiconductor NWs have the advantage as NWs, comparing to their bulk counterparts. For instance, they have high crystallinity because the lattice mismatch issue during growth process is relaxed much. For epitaxial growth of NWs, the mismatch tolerance can be as large as 8%[2], which is not allowable for growing high quality wafers. Thus the limitation for substrate or heterostructure with some specific materials (that have relatively large lattice mismatch while important for application, such as InAs and InP NW heterostructures[3]) can be removed. This can open new paths and may lead to better electronic and optical properties. Moreover, the cost is reduced since the consumption of material is less. This reveals a potential for large-scale industrial production purpose.

Currently speaking, semiconductor NWs have been applied to different aspects such as lasers[4], light-emitting diodes[5], solar cells[6], logic gates[7], photo-detectors[8], waveguides[9], biological and medical sensing[10] etc. These applications show the versatility of NW and its potential for electrical and optical engineering for future technology.

1.2 Purpose of This Paper

There are many ways for synthesizing NWs, top-down approach such as lithography or electrophoresis, or bottom-up approach such as electrochemical deposition, vapor deposition, or vapor-liquid-solid (VLS) growth. Though these methods have been studied and used much, a basic understanding of efficiency about photo-conversation based on the quality of semiconductor NWs is still not understood. In particular, the quantitative information about this quantum efficiency (QE) is inadequate while it is an important value to assess the quality of NWs in terms of optical characteristic.

For example, our group uses chemical vapor deposition (CVD) method to grow many kinds of nanowires such as II-VI group materials CdS and CdSe, or erbium chloride silicate (ECS). The following characterization will be done with scanning electron microscope (SEM) or transmission electron microscopy (TEM). For the optical properties, the photoluminescence (PL) measurement is carried out to check the light emission intensity. Though these procedures are useful for evaluating the quality of grown NWs, there is not a method to represent it quantitatively. Moreover, the absorption of NWs is not counted into so that a strong PL emission does not necessarily stand for a good quality. Thus this paper will focus on the measurement of QE value of NWs to achieve these purposes, especially for semiconductor alloyed NWs, with different alloy

composition and excitation intensity.

2. Recombination Process

Due to my research area here, it is necessary to talk about what is QE in semiconductors first, which relating much with different recombination process for excited carriers within conduction band and valence band. Generally speaking, the recombination process can be divided into radiative and non-radiative paths, which has emission of photons or phonons (in most cases) respectively. This requires the initial system to be not under equilibrium condition, which in other words, some form of excitation that can generate a high concentration of electron-hole pairs, is needed for recombination to take place. The excitation source can be electrical (which results in electroluminescence), optical (which produces photoluminescence), or with an electron beam (or so-called electron bombardment that causes cathodoluminescence).

Considering for most cases, radiative transitions can be treated as the opposite direction of absorption processes. However, there is an apparent and significant difference between the two. The absorption can relate to all states in the semiconductor, which leading to a broad emission spectrum. In contrast, its counterpart involves a narrow band of states containing the thermalized electrons and holes which causes a much narrower spectrum.

What's more, during recombination, the intermediate states can contribute to either radiative or non-radiative process while absorption does not take them into account. Consider the model below (Figure 1), where u, l, and i represents upper-level, lower-level, and intermediate state respectively.

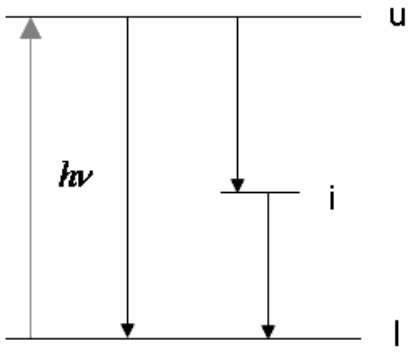

Figure 1 Model of intermediate states

It is apparent that only l→u is involved in absorption, while both processes u→l and u→i→l are considered to be the available recombination channels and competitive with each other. The latter process, if is radiative, will produce photons with energy less than hυ. Assume recombination time for these two is τ and τ´ each, now we can find the effective recombination time can be expressed as[11]:

$$\frac{1}{\tau_{eff}} = \frac{1}{\tau} + \frac{1}{\tau'}$$

And the radiative efficiency is then:

$$\eta = \frac{\text{radiative recombination rate}}{\text{total recombination rate}} = \frac{1/\tau}{1/\tau_{eff}} = \frac{1}{1+\tau/\tau'}$$

So next I will discuss several basic transition mechanisms for both radiative and non-radiative paths.

2.1 Radiative Recombination

2.1.1 Band to Band Transitions

The most common and known process is the recombination of excited electron-hole pairs as free carriers. For direct and indirect semiconductor, the transition can be indicated below respectively.

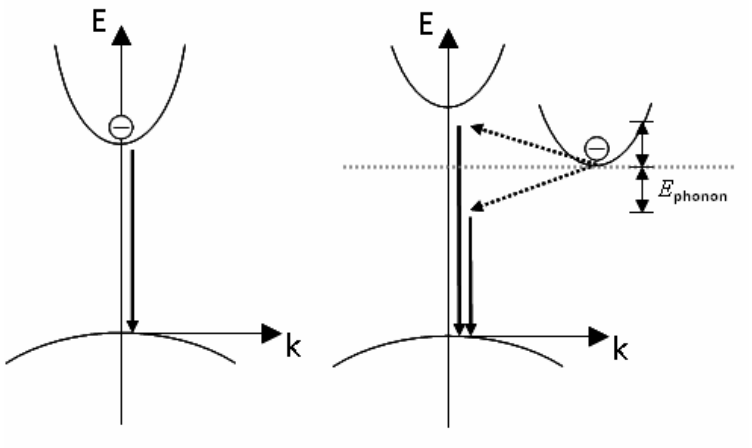

Figure 2 Band-to-band radiative transitions in k space

One thing should be clarified though is that since a photon has very small momentum; the process which emits a photon performs a vertical transition in k (wave factor) space.

For direct bandgap materials, since the maximum of valence band and the minimum of conduction band are close to have same k values, the transition is initially momentum conserved. With increasing excitation rate or the

temperature, deeper states in the band will be filled in, which introducing emission with higher photon energy. This is so-called band filling and represented by a blue shift from PL spectrum.

For indirect bandgap materials, however, since the extrema of two bands do not have same k values, the transition needs to be assisted by phonons. There are two ways for fulfilling this: phonon-absorption and phonon-emission, as we can see from Figure 2. Usually the latter one will be mostly the case. This is because the number of phonons which are available for absorption is small, especially at low temperature, while the emission of phonons is more possible since many electrons are already occupying high energy states. What's more, the photon energy needed with phonon-emission is smaller with a minimum energy equals to E_g-E_p, while with phonon-absorption the photon energy needs to be at least E_g+E_p, which may be more easily reabsorbed by the material itself.

2.1.2 Free-to-bound Transitions

At higher temperature, band-to-band transitions usually dominate since the impurities (the shallow ones) are ionized. This will change at lower temperature, when the carriers are bounded with impurities. For instance, the free electrons in the conduction band can recombine with the holes which are trapped on the acceptors. The emitted photon will have energy written as E_g-E_A, where E_A is the binding energy of acceptor. With increasing acceptor

concentration, the wavefunction of them will begin to overlap as they are closer to each other. Thus the acceptor level changes to an impurity band. It will further overlap with the valence band so that holes are free again. This PL intensity will change with temperature as $1-\exp\left[-E_A/\left(k_BT\right)\right]$ [12].

2.1.3 Donor-acceptor-pair Transitions

Consider a semiconductor with both donors and acceptors. Under thermal equilibrium conditions, some electrons from donors will be captured by the holes in acceptors, which form a so-called compensated semiconductor, that have both ionized donors (D^+) and acceptors (A^-). Excess free electrons and holes in the conduction band and valence band via optical excitation can be trapped into those ionized states and produce neutral D^o and A^o centers. Then these electrons and holes will recombine radiatively. This process can be expressed as follow:

$$D^0 + A^0 \rightarrow \hbar\omega + D^+ + A^-$$

During such donor-acceptor-pair (DAP) transition, one may intuitively assume that the emitted photon will have energy as:

$$\hbar\omega = E_g - E_A - E_D$$

However, considered the coulomb interaction between the ionized donors and acceptors, this energy should be modified to[12]:

$$\hbar\omega = E_g - E_A - E_D + e^2/\left(4\pi\varepsilon_0\varepsilon R\right)$$

2.1.4 Exciton

Consider the correlation between excess electrons and holes in the conduction band and valence band this time, which are neglected in band-to-band transitions. At low temperature or the material is very pure with few defect or trap states, the coulomb attraction within a free electron and a free hole is needed to be concerned. Thus the electron will orbit around the hole acting as a hydrogen atom system. And the ionization energy for such a system can be written as:

$$E_x = \frac{-m_r^* e^4}{32\pi^2 \hbar^2 \left(\varepsilon_0 \varepsilon_r\right)^2} \frac{1}{n^2}$$

where n is an integer indicating the various exciton states and m_r^* is the reduced mass which can be represented by effective masses of electron and hole by m_e^* and m_h^* respectively:

$$\frac{1}{m_r^*} = \frac{1}{m_e^*} + \frac{1}{m_h^*}$$

Though the exciton states do not have a defined potential in the band diagram of semiconductor, it is usually assumed that the conduction band edge is a reference energy level as continuum state, which stands for n=∞.

With increasing temperature that is higher than the ionization energy, the exciton will dissociate and become free electron and hole again. At room temperature, which has thermal energy kT ≈ 26 meV, is high enough to ionize

most kinds of exciton. Thus exciton usually cannot exist in room temperature. It is worthy to mention, within the group of II-VI semiconductors, bulk CdS has a relatively high exciton binding energy of 27meV[13]. If the purity is high and it has few defects or trap states, the excitonic effect can still be observed at room temperature.

As illustrated in Figure 3(a), the exciton can recombine and emit photons with energy $h\nu = E_g - E_x$ in direct gap material. Other emission lines with $E_g - \left(1/n^2\right)E_x$ (n>1) are usually hard to observe with other near-bandgap radiative processes.

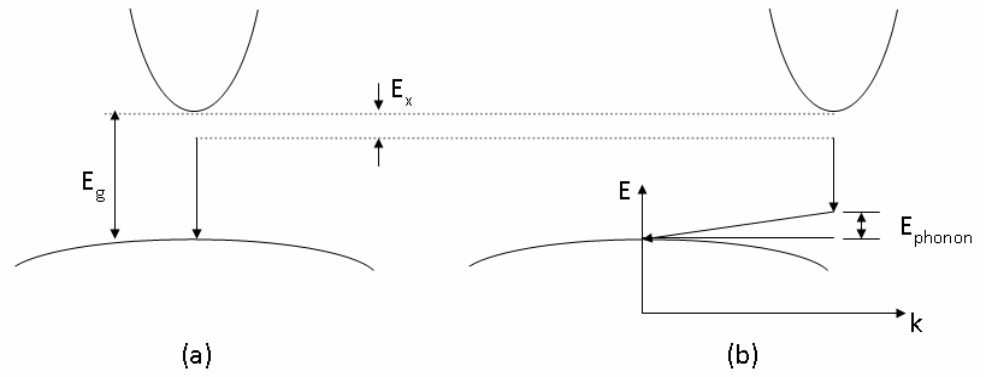

Figure 3 Free exciton recombination in k space

For indirect gap semiconductors, due to the necessity for momentum conservation, the energy of photons emitted is $h\nu = E_g - E_x - E_p$. Actually even for direct transition like Figure 3(a), the emission with one or more longitudinal optical (LO) phonons (the possible ones at k=0, with the energy of ~0.038eV) can also occur. Thus the exciton emission spectrum will have several replicas

with photon energy $h\nu = E_g - E_x - mE_p$, where m is the number of emitted LO phonons from one recombination process.

At high carrier concentration, electron and hole repulse with themselves and try to reduce the range where attractive coulomb interaction can take place, which is so-called screened coulomb interaction, thus leads to reduction of excitonic effect.

The description above is for free excitons. With increasing excitation, the mechanism becomes more complicate due to the exciton interacting with another exciton(s), donor, and acceptor, which can be named as excitonic complexes. These emissions can be observed at usually sufficient low temperature.

2.2 Non-radiative Recombination

Non-radiative recombination is another important transition process for semiconductors. In fact, it is the dominant process for some semiconductors or in some specific conditions. Compared to radiative recombination, the non-radiative one indicates any process that does not emit photons, but rather phonons, or equivalent for lattice vibration, in most cases.

2.2.1 Auger Effect

Perhaps Auger effect is the most known process for non-radiative recombination. During the process, the energy release by the first electron recombined is absorbed right away by the second electron in the conduction band (or donor level) to go into higher states. Then this electron will dissipate its energy by emitting phonons. Therefore it is a three-particle process. Some representative configurations are shown below.

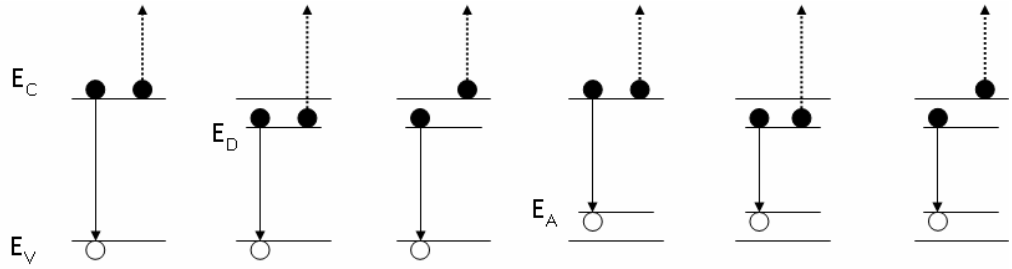

Figure 4 Diagram of Auger process for n-type semiconductor

The figure here is for n-type materials only though the p-type one can be similarly depicted out. Since it is a carrier-carrier interaction, it is obvious that Auger effect will become more important with increasing carrier density. With this judgment, increasing temperature will facilitate this effect also since the carrier density increases with temperature as $\left(kT/E_g\right)^{3/2}\exp\left(-E_g/kT\right)$. Thus for small bandgap materials, this process will be strongly temperature-dependent, and more likely to take place since it is easier for momentum conservation during the transition.

2.2.2 Surface/defect-related Recombination

Other than Auger process, another significant aspect will relate to surface states and defects, or so-called Shockley-Read-Hall (SRH) recombination. Usually a surface state corresponds to a dangling bond which can absorb impurity from outer environment such as oxygen. The defect state, however, can be treated as an internal surface state. They may be important especially for NWs due to their larger surface-to-volume ratio comparing to bulk materials. What's more, the defects which are originally within the bulk semiconductor may become surface states due to this ratio. Such characteristic implies that surface passivation will well improve the performance of NWs and its application such as solar cells[6].

3. Internal Quantum Efficiency and Measurement

From above, we can generally write the rate of recombination processes for photo-generated carriers as follow:

$$\frac{dn}{dt} = -\left(An + Bn^2 + Cn^3\right)$$

where A, B, and C represent the SRH, radiative, and Auger process respectively. Thus the internal quantum efficiency can be written as:

$$\eta_{\text{int}} = \frac{\text{No. of generated photons}}{\text{No. of absorbed photons}} = \frac{Bn^2}{An + Bn^2 + Cn^3}$$

Now I will discuss a relative measurement method, which was done on

InGaN/GaN wafers for GaNotech®. It is based on 2 major assumptions:

1) Extraction efficiency remains the same under different temperatures.
2) IQE will be unity at sufficient low temperature, i.e. liquid helium temperature.

The PL signals for the sample are measured at 5K, 77K and 300K respectively. The rate equation can be written as:

$$\frac{dN}{dt} = -\left(AN + BN^2 + CN^3\right) + \alpha P_{pump}$$

where P_{pump} is the laser pumping power density. In steady state, $dN/dt = 0$, so we can get

$$\left(AN + BN^2 + CN^3\right) = \alpha P_{pump}$$

The detector records the integrated PL intensity $I = k \cdot BN^2$, where k is the extraction efficiency. Thus the IQE can be calculated from following equation:

$$\eta_i = \frac{BN^2}{AN + BN^2 + CN^3} = \frac{I}{k} \cdot \frac{1}{\alpha P_{pump}}$$

By using the assumptions, $k = const.$ and $(\eta_i)_{5K} \approx 1$ is valid during the measurement, so that we can get IQE at $T = 77K$ or $T = 300K$.

$$(\eta_i)_T = \frac{\left(I \big/ \alpha P_{pump}\right)_T}{\left(I \big/ \alpha P_{pump}\right)_{5K}}.$$

This method is relatively simple, though its validity will mainly rely on the assumptions. For the first one, the temperature variation may change the

transmission and reflection of the materials, which may lead to different k .

For the second assumption, IQE is assumed to be 100% at very low temperature. However, the IQE, or the corresponding PL intensity, is still dependent on carrier density even at low temperature, which means the non-radiative, radiative and Auger processes are still valid[14]. Therefore, a range covering several orders of magnitude of excitation power densities will be needed to examine the peak IQE at $T_0 = 5K$, which will be the exact value for the calculation in denominator.

What's more, the absorption will actually change with temperature under same excitation, due to bandgap of the material is shifted, which is illustrated below.

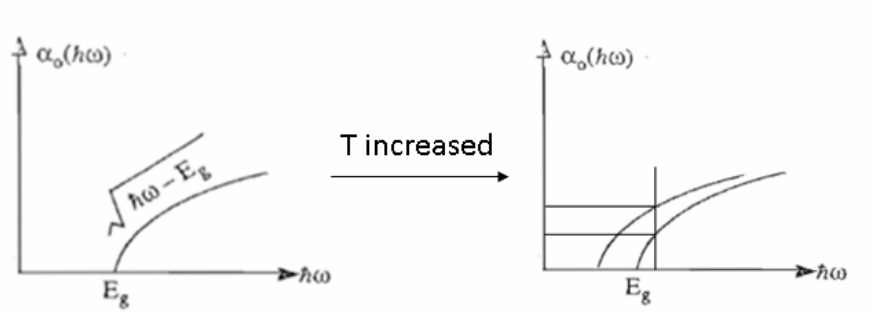

Figure 5 Absorption difference with temperature under same excitation

4. Photoluminescence Quantum Efficiency Measurement

The method we introduce here is generally based on John C. de Mello's paper[15], which is combined with photoluminescence (PL) measurements and an integrating sphere. Before describing this approach, it is necessary to introduce

this sphere first plus the reason we use it.

4.1 Integrating Sphere

4.1.1 Theory

The integrating sphere is useful and common equipment for measurement of reflectance or transmittance flux from diffuse or scattering materials[16]. It is used for spatially integrating the radiant flux. There are two crucial parameters for this instrument named sphere multiplier and the average reflectance.

To begin with, the radiance L of a diffuse surface for an input flux Φ can be written as $L = \frac{\Phi\rho}{\pi A}$, with unit to be W/m²/sr. Here ρ is the reflectance, which usually is in the range of 0.94 ~ 0.99 for real integrating sphere. A is the illuminated area while π is the total projected solid angle from the surface.

Consider the situation below (Figure 6), the flux incident on the entire sphere can be expressed as $\Phi\rho(1-f)$, where f is the total port fraction of the sphere. Like the figure below, which containing 2 ports, then f is the total port area divided by the total sphere area (including port). For a designed sphere, the port fraction f is usually very small, between 0.02 ~ 0.05. One thing need to clarify is that it is assumed that there is no reflection (ρ→ 0) from a port area.

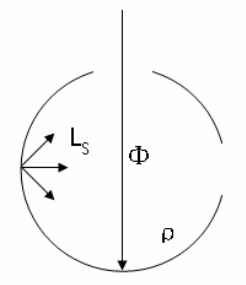

Figure 6 Radiance in a sphere

After the second reflection, it is easy to find the flux now is $\Phi\rho^2(1-f)^2$, with watt as unit. Therefore after n reflections, the total amount of flux can be represented as $\Phi\rho(1-f)\left[1+\rho(1-f)+...+\rho^{n-1}(1-f)^{n-1}\right]$. If n goes to infinity, noticing this will be an infinite geometric series if $\rho(1-f)<1$, which is the case here since both numbers are less than 1, its sum can be written as $\frac{\Phi\rho(1-f)}{1-\rho(1-f)}$. Thus the radiance of the surface from the sphere is:

$$L_s = \frac{\Phi}{\pi A_s(1-f)} \cdot \frac{\rho(1-f)}{1-\rho(1-f)} = \frac{\Phi}{\pi A_s} \cdot \frac{\rho}{1-\rho(1-f)}$$

The first part of the equation is almost the same with $L = \frac{\Phi\rho}{\pi A}$, the radiance of a diffuse surface; while the second part is unitless and is defined to be the sphere multiplier M, which accounting for the level of multiplication after many times of reflection in the sphere. The figure below illustrates the correlation among M, ρ and f.

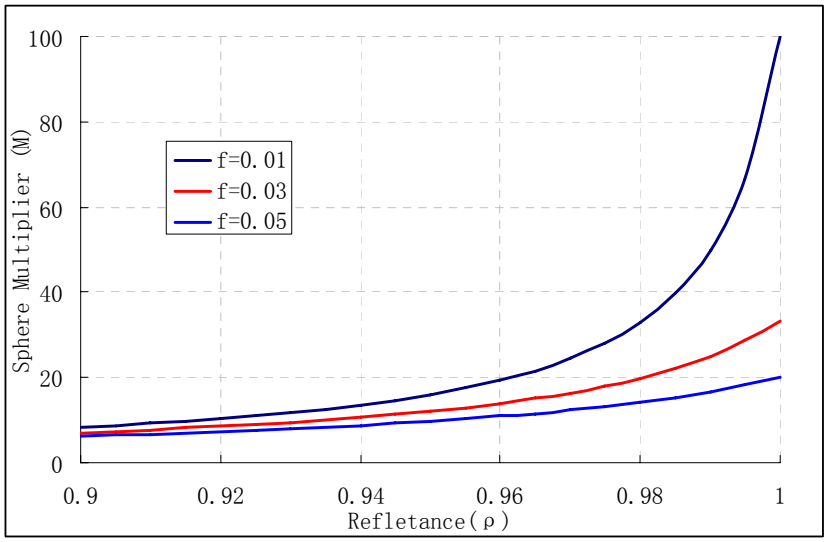

Figure 7 The sphere multiplier M and its factors

For sphere in reality, as mentioned before, with reflectance between 0.94 ~ 0.99 and port fraction between 0.02 ~ 0.05, the sphere multiplier is about 10 ~ 30.

When it comes to the practical design, the sphere diameter is also another important parameter. In general, though the smallest sphere can produce the highest radiance, a larger diameter with smaller port fraction improves the spatial performance since the function for an integrating sphere is to spatially integrate the radiant flux inside it. Also a high reflectance coating can help achieving this, which will be mentioned shortly. Another way is to add baffles with same coating inside the sphere, which prevent any flux that incident into the exit port directly or with less than two times of reflection.

4.1.2 Description of Customized Sphere

For our experiment purpose, since the sample will contain bunch of NWs on the surface of it, the radiant light reflected or generated from sample will be much scattered. Therefore it is not accurate to measure the exact intensity of emission from a specific orientation, e.g. specular reflection direction, especially for quantum efficiency measurement. So that it is suitable to utilize an integrating sphere to obtain the precise signal intensity for both laser and PL emission.

The integrating sphere we use here is bought from Labsphere®. It is a customized sphere with 6 inch interior diameter based on Model RTC-060-SF (Figure 8).

Figure 8 Standard integrating sphere RTC-060-SF from Labsphere®

According to our design, the sphere will have 4 ports as drawn in Figure 9.

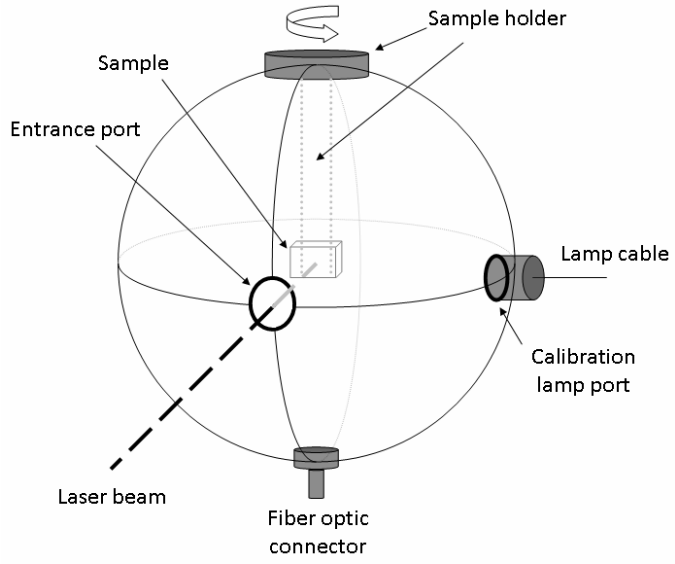

Figure 9 Schematic of customized integrating sphere

There is a detection port at South Pole of the sphere with SMA fiber adapter, which is then connected to the spectrometer via fiber optic. The port at North Pole is made for accepting the center mount sample holder. The holder has an external control and the position of it can be adjusted. So that laser will incident onto the sample directly or not. The 0.25 inch entrance port at 0° is for illumination, e.g. laser excitation for our measurements. The 1 inch port at 90° is to accept calibration lamp, which will be discussed later.

A very important part for an integrating sphere is the reflectance coating on the surface of interior sphere. Spectralon® and Spectraflect® are two known effective diffuse reflectors offered by Labsphere®. They are both applied to 250nm to 2500nm range, which cover the UV-VIS-NIR region. The reflectance

response versus wavelength can be seen below:

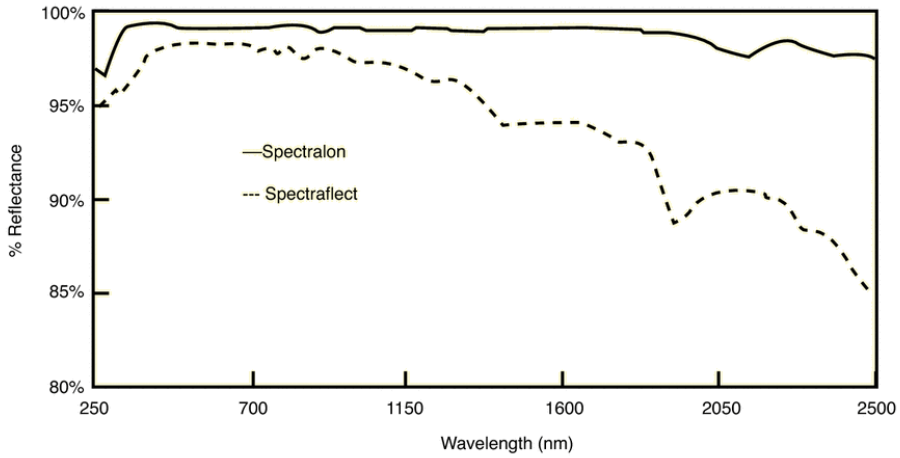

Figure 10 Reflectance response for two coating materials

Here we use the Spectralon coating for best reflectance result. It is a fluoropolymer and has the highest diffuse reflectance of any known material within above range. It has >99% reflectance from 400~1500nm and >95% from 250~2500nm[17] and performs a high Lambertian behavior which is ideal for integrating sphere coating.

4.2 Experiment Method

The experiment is separated into three different steps/configurations, as indicated in Figure 11:

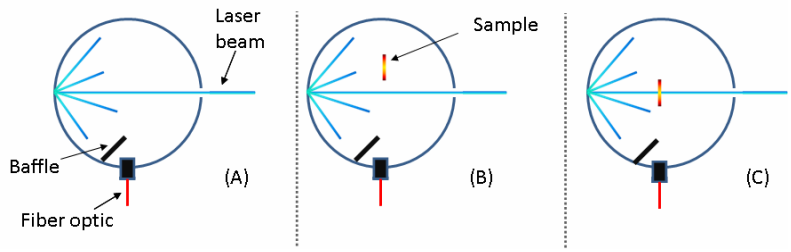

Figure 11 Schematic for PLQE measurement based on 3 configurations

In each configuration, the laser beam will incident into the integrating sphere with a small entrance port. Regardless there is a sample or not in the laser path, laser will scatter in the sphere. The total signal from laser and/or sample will be collected by a spectrometer through fiber optic.

The first graph of Figure 11, or experiment (A), will measure the laser and background signal in the sphere. Even though we will not put the sample inside the sphere now, the empty sample holder should be settled inside at the beginning to maintain the same background condition during the measurements.

The experiment (B) and (C) will measure the laser and also PL signal from sample. The difference lies in whether the sample is in the laser path or not, as shown in the third graph of Figure 11. In other words, the PL emission signal from experiment (B) will only be generated from scattered laser, while the experiment (C) will have PL signal from both scattered and also directly incident laser light.

For notation, the laser signal will use L and the PL signal will be P. For instance, the signal collected via system from configuration (C) will be L_c and P_c respectively. In configuration (B), a small fraction μ of laser power will be absorbed by the sample after being scattered in the sphere. So that

$$L_b = L_a\left(1-\mu\right)$$

In configuration (C), laser hit the sample directly and a fraction A of it will be absorbed by the sample first. After that, the transmitted or reflected laser will be scattered in the sphere, which is again similar with the set-up (B) condition. Therefore, we will have

$$L_c = L_a\left(1-A\right)\left(1-\mu\right)$$

This can reveal A, which indicating the absorption of incident laser light from sample.

$$A = 1-\frac{L_c}{L_b}$$

The signal colleted from (C), which is $L_c + P_c$, should be divided into 2 parts. The emission generated from directly incident laser light can be written as $\eta L_a A$, where η is the photoluminescence quantum efficiency (PLQE) that we want to measure eventually. It is defined as

$$\eta = \frac{\text{number of photons emitted}}{\text{number of photons absorbed}}$$

The unabsorbed laser power will be absorbed by the sample again after being scattered. Since we already get the total signal $L_b + P_b$ from configuration (B), this part can be given by $\left(1-A\right)\left(L_b + P_b\right)$.

By summarizing all above, we can derive the relationship with PLQE as follow:

$$L_c + P_c = \left(1-A\right)\left(L_b + P_b\right) + \eta L_a A$$

$$\Rightarrow \eta = \frac{P_c - (1-A)P_b}{L_a A}$$

It is necessary to mention that the above statement is based on the assumption that there is no noticeable difference where the laser is first scattered on the sphere inner surface.

4.3 Experiment Setup

The experiment setup based on above method is shown:

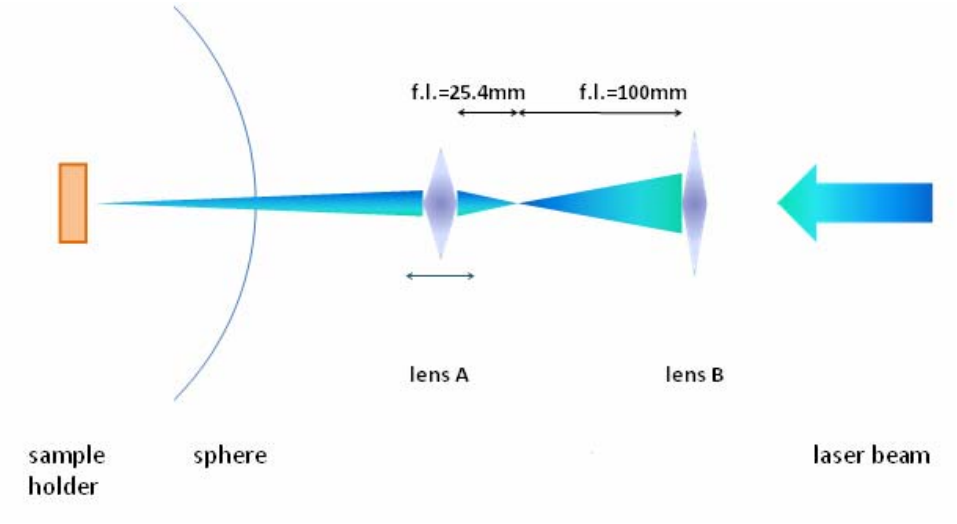

Figure 12 Schematic for experiment setup

The excitation source we use is the Ti: Sapphire laser (Tsunami®, pumping with a 532nm Millennia® laser) which operates at around 795nm range. For photoluminescence emission purpose, the laser beam is modulated under second harmonic generation (SHG) and emits at 395nm. This laser output at the entrance of sphere (the actual power for excitation) is about 150mW. The laser spot size is around 0.5mm in diameter after the beam is adjusted to focus

on the sample. Therefore, the excitation density for this laser beam will be about 70W/cm^2. Though it is only an approximation since we cannot get a precise image of the laser spot size on the sample surface from camera, the order of magnitude of excitation density should be within the range of 10^2W/cm^2.

The lens A and B are used for beam size shrinking. Their focal lengths are 25.4mm and 100mm respectively, which means, if their distance is 125.4mm, the collimated beam size will be about 1/4 of the original one. Then, by adjusting the position of lens A horizontally along the direction of beam path, as indicated from Figure 12, we can control the spot size of laser beam on the sample. Namely, if the lens A is moved toward lens B, the focal point will be virtual one and spot size will be enlarged; on the other hand, if the lens A is moved away from lens B, the spot size will be smaller and will finally become focused.

4.4 Sample Preparation

4.4.1 Growth process

The cadmium sulfide selenide ($CdS_xSe_{(1-x)}$) alloy NWs are grown by our previous group members[18]. For the integrity of this thesis, the growth process will be briefly introduced here. The growth method, as mentioned previously, is chemical vapor deposition (CVD). The furnace setup and tube configuration, though is not totally the same, can be illustrated as Figure 13 below[19].

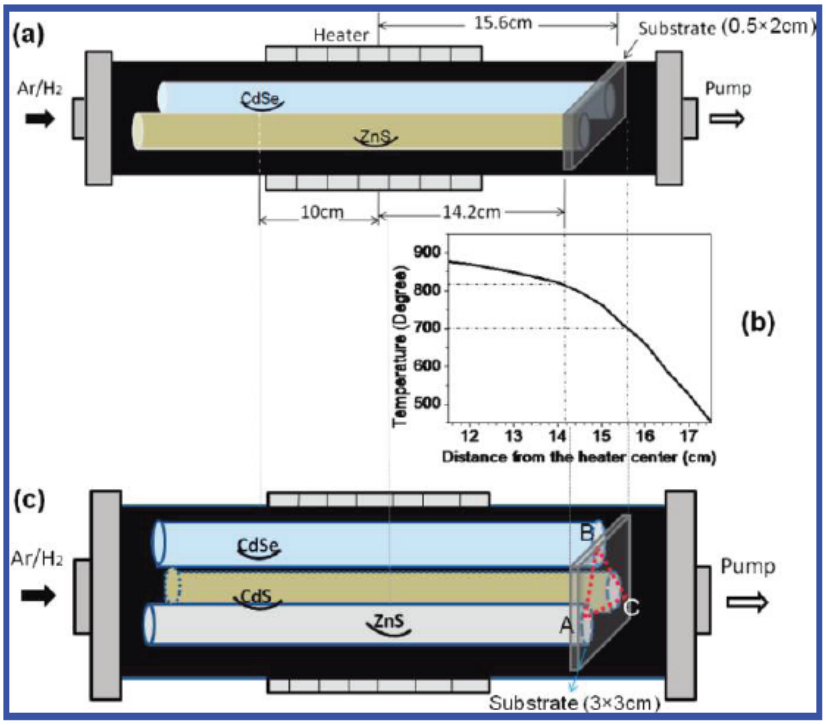

Figure 13 The growth process setup and tube configuration

Here (a) and (c) are representing the growth of quaternary ZnCdSSe alloy NWs on 1D and 2D graded sample and (b) is the temperature profile at the substrate. The growth of ternary CdSSe alloy NWs has similar setup as Figure 13(a) though ZnS powder is changed to CdS one.

The grown samples show good spatially composition-graded NWs, as can be seen from Figure 14[18].

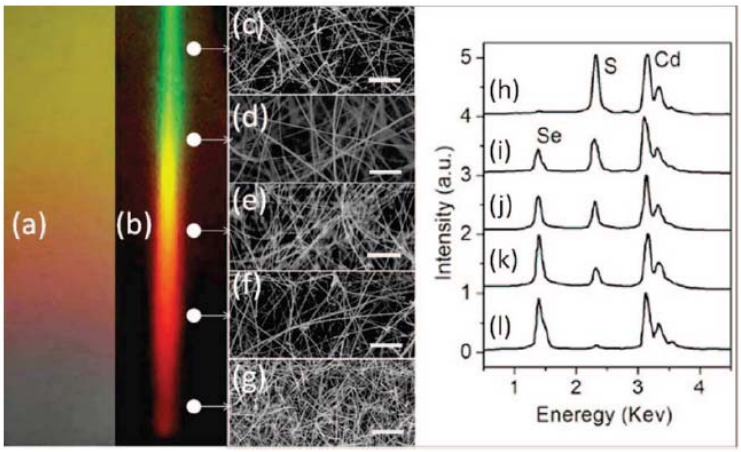

Figure 14 Spatially composition-graded CdSSe NWs on a quartz substrate

The figures (a) and (b) are real-color images under room lighting and 266 nm laser illumination. Pictures (c) to (g) are SEM images from white spots of (b), respectively, with scale bar to be 5 μm. The right figure is energy-dispersive X-ray spectroscopy (EDS) images corresponding to (c) to (g) spots. Here we can see our group successively synthesize this kind of NWs on a single substrate.

For measurement purpose, two samples were chosen: sample A is with silicon substrate, while sample B is with quartz substrate. Though there should be no apparent relationship with different substrates for samples in terms of NWs' quality and PLQE, the NWs from these two samples were still dispersed onto clean glass to avoid impact from substrate, which later we found is important to get accurate quantum efficiency result, particularly for sample A with silicon substrate. This will be mentioned in the measurement chapter for detailed illustration.

4.4.2 Dispersion

Dispersion is an easy while important approach for NW characterization, especially for single NW. First a VWR* Micro Cover Glass (Square, No.1) is cut into many small pieces. The ones with area around 500mm×500mm are chosen and isopropanol (also called isopropyl alcohol) is dripped onto them. After that, put one small glass onto the as-grown sample and press it for 1~2 seconds. Then we get a bunch of NWs on a small piece of glass. It is convenient and effective; since many dispersed samples can be made and tested at one time, which is suitable for a series of experiments such as power-dependence measurements or large amount of samples to be tested, plus we do not require single NW measurement.

However, this procedure will cause the layer thickness of dispersed NWs to be different (from monolayer to several monolayers), which leads to different absorption of light and successive emission intensity. What's more, the number of NWs in the laser spot is different from each other, which leads to different emission intensity also for same position of as-grown sample. Even though, these problems can be dealt with since the absorption will be measured. Based on the assumption that the number of excited NWs is proportional to absorption, this method is reasonable.

4.4.3 Photodegradation

After the system was built up and samples were ready, when the initial test started, a phenomenon of PL emission decreasing with continuous laser illumination had been observed. It exists throughout all the experiments we have done and only differ with how fast it behaves. A typical trend is plotted in Figure 15. For convenience, only peak intensity of PL emission has been recorded, and points are taken for each other 5 seconds.

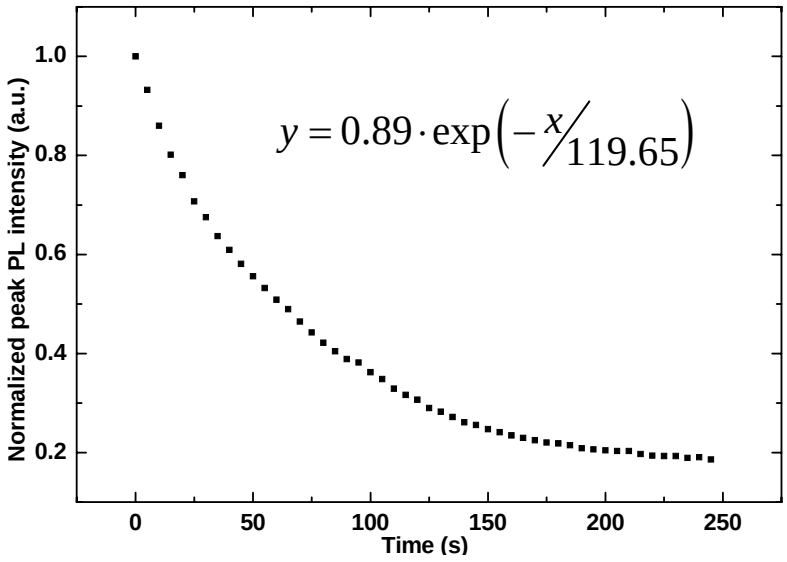

Figure 15 Decrease of PL intensity with continuous laser illumination

From the figure we can see the peak emission dropped 14% for first 10 seconds, or 24% for first 20 seconds. The function inside the figure is obtained by using plot fitting function from Origin 8 program. As have mentioned, the rate for such decreasing varies for different samples.

Such PL decreasing will reduce the measured emission signal from detector and

eventually leads to underestimating the PLQE of NWs. Therefore we need to find out what causes such effect and how can it be prevented.

First we find this phenomenon will be continuous only under laser irradiation. In other words, say, if laser is blocked from sample by shutter for 60 seconds (no laser signal interact with sample), which considerable PL decreasing with laser illumination should be observed, there is no decrease of such within this period. And after this 60 seconds, when shutter is open again and laser is incident onto sample, the PL signal drops from the point when laser was blocked 60 seconds ago. Thus we can say this non-recoverable phenomenon has direct relationship with laser effect, which can be the light pressure generated on the sample surface, the localized heating at and near laser spot, or the degradation of NWs' quality. The last one is confirmed from our later power-dependence measurements and therefore this PL decreasing phenomenon can be called photodegradation as described in literature[20].

However, at the beginning, we assume this is only due to the weak force that connects dispersed NWs and glass substrate. We believe the bounding force is mainly from the Van der Waals force. Since the sample is vertical placed, the gravity of NW already gives itself some degree of unstable initially. When irradiation is introduced, the weak force is influenced by the generated light pressure and result in the NWs being pushing away from the laser spot (which

decrease the total emission from this spot) or even dropping off from the glass substrate.

Therefore we need to find a way to stabilize the dispersed NWs from moving around. Here we use a kind of glue ("Ace" Marine® Epoxy 0.85 oz) to stick two glasses (one is the original small piece of glass with dispersed NWs and one is a larger piece used as substrate, as drawn in Figure 16) together with NWs between them, which acts like a sandwich structure.

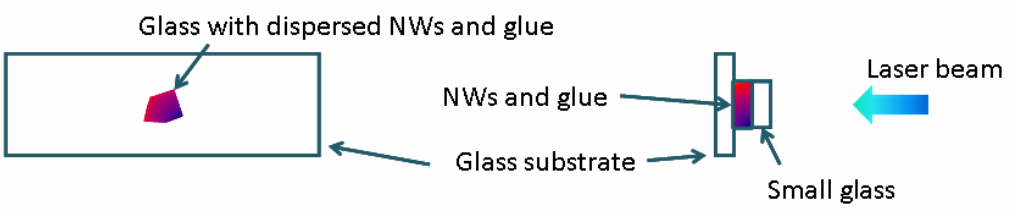

Figure 16 Dispersion process with glue

The glue is uniformly distributed between two glasses also so that now the NWs and glue are mixed together. It is important to note that the glue has no chemical or physical interaction with NWs. From the experiment, though the glue will absorb a small portion of laser intensity (from 3%~5%), it does not generate any noticeable emission within detection range.

Then next we need to examine if it can solve the problem. A sample with dispersed NWs was tested for the peak PL emission intensity and then we used the glue to stick it with a larger cover glass and tested again. The result is plotted below.

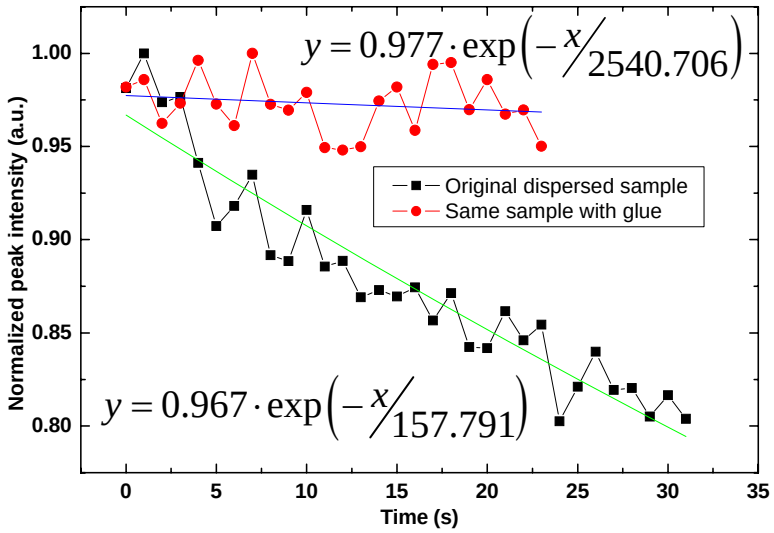

Figure 17 Comparison the degradation effect with and without glue

The black and red dots are the recorded PL signal (peak only as the same with previous figure for 1 second between each) for these two samples as mentioned above. The green and blue lines are fitting curves respectively with fitting functions given. From this figure we can see the sample after such process reduces the photodegradation much. The only thing we need to clarify here is the absorption layer thickness is increased compared to original dispersed sample. Thus such additional absorption of laser excitation needs to be considered during PLQE calculation, which is L_c specifically saying.

Though seems like the phenomenon has been improved much, it is not totally prevented. In fact after testing many samples undergone this process, we find such photodegradation is still noticeable after a time period, e.g. a few tens of seconds, of illumination from laser. Since the processing above should be

able to stop NWs from moving around, there could be other responsible factors for such degradation, which may be referred to the additional recombination process in the NWs or the local heating in and near the excitation spot. So during the power dependence measurements, this issue will be looked into again and we find the photodegradation is dependent with the excitation density, which clearly shows the recombination process is involved in.

Anyhow, since the degradation can be reduced for some degree, such process employed to all latter dispersed samples under measurement to approach more accurate quantum efficiency result, if not stated specifically.

4.5 Measurement

4.5.1 Wavelength-dependence Measurement

At first the as-grown samples are used for measurements. Sample A with silicon substrate is chosen to be tested first. Since our $CdS_xSe_{(1-x)}$ NW samples have spatial gradient change of mole fraction x from 1 to 0 along one direction, the peak position of PL emission shifts from green (CdS rich part) to near-infrared region (CdSe rich part) during the scan from one side to the other of the sample, as shown in Figure 18.

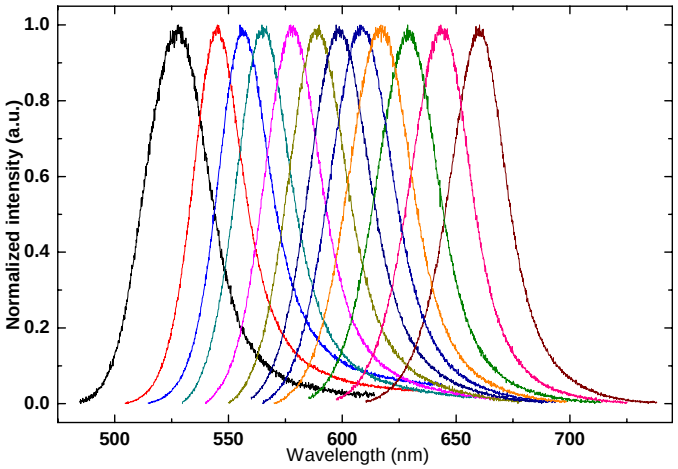

Figure 18 PL emission from alloy $CdS_xSe_{(1-x)}$ NWs sample

This is consistent with the one from previous introduction of such alloy NW samples. After the initial scan, next step we try to calculate its PLQE following the procedure introduced previously. The collected signals are shown in Figure 19 as an example. The left hand side contains laser signals from three configurations, while the PL emission signal from one spot of sample A is on the right hand side.

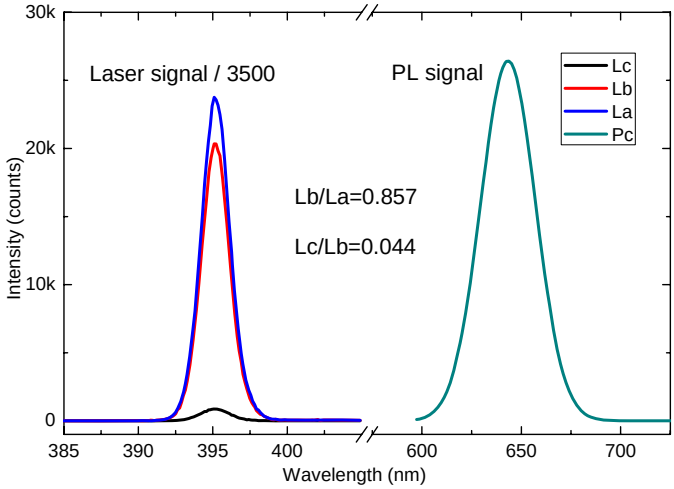

Figure 19 The PL spectra from as-grown sample

We can see from the figure that the laser signal is absorbed by 14.3% (1-0.857=0.143) with configuration B, and by 95.6% (1-0.044=0.956) with configuration C. It shows that the absorption from as-grown sample with silicon substrate is very large (A>95%) and it is common for all spots measured with this sample.

Here it is necessary to mention that due to strong intensity from laser power, a filter with optical density (OD) 3.0 (from Newport® FS-3 Filter Set) is used before the spectrometer. Usually the definition is OD=-log (T) where T is transmission that within range 0 ~ 1. Thus OD3.0 corresponds to a transmission T=0.001. However, since its usual wavelength range is 400 nm ~ 900 nm, the transmission changed a bit at 395 nm, which is not $1/10^3$ any more, but rather $1/3500=2.86\times10^{-4}$ in average (Figure 20). It is achieved by using the calibration lamp and calculated by with and without filter. The actual spectrum response for OD3.0 filter near 395nm range can be seen below. After all, this factor needs to be concerned in the calculation for L_a.

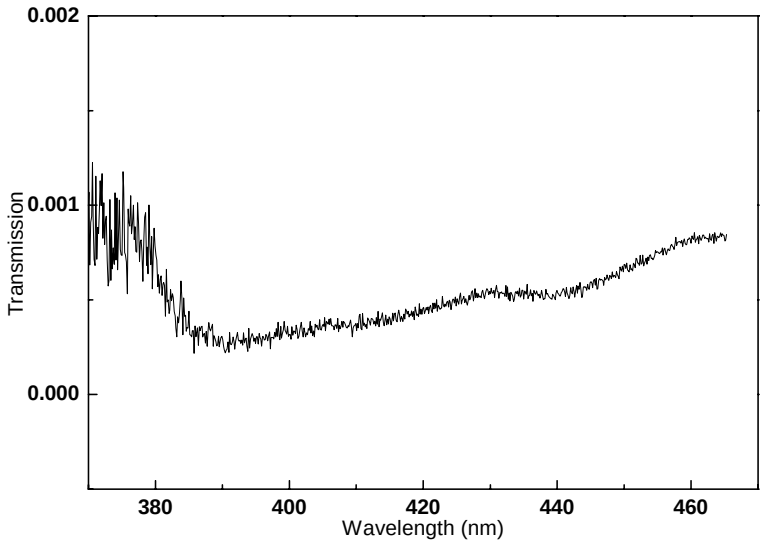

Figure 20 The spectral response of filter

For all spots measured here, the PLQE calculated is in the range of 0.04% to 0.09%, which is very small and not reliable since the reported quantum efficiency is ranging from 0.1~20%[21]. This is because we overestimated the absorption and we believe there are two possible factors should be responsible for it.

One is that the silicon substrate will absorb the incident and scattered laser power in the sphere and has an emission out of the detection range. It results in a much smaller value of L_c collected from the detector, which in turn, a much larger absorption A.

The other possible reason is that since the NWs on as-grown sample are entangled or stacked together with each other, they will form a thick layer and thus absorb much more laser power density and also cause self-absorption of

successive emission from NWs themselves. This situation will decrease P_c and L_c at the same time, which also leads to underestimated PLQE result. Such effect has been illustrated from literature[22] with Figure 21.

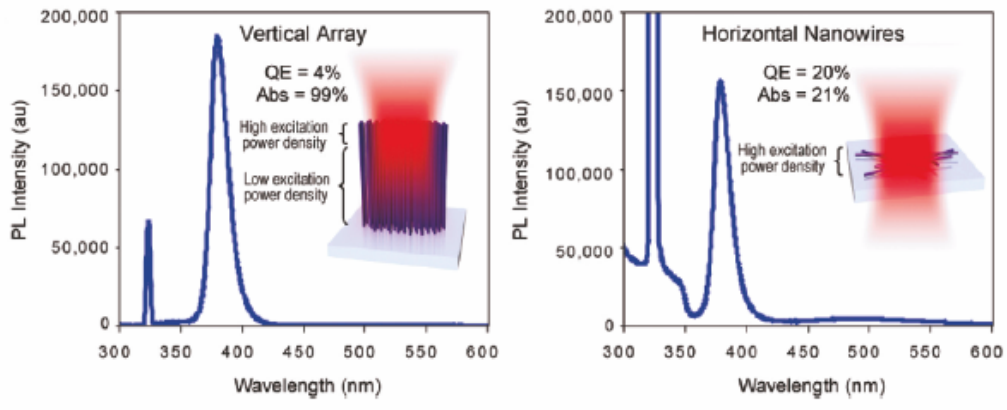

Figure 21 The absorption divergence for different orientation of NWs

From the above figure we can see the absorption of NWs will be very large (99% here) if the laser undergoes a long path within NWs. Otherwise, with dispersion procedure, since the NWs are scattered on the new substrate, the absorption decreases much (21% from the figure) and leads to a more accurate value of PLQE.

From our observation and the literature, it is necessary to use dispersed samples for a more appropriate approach. By doing this, the silicon substrate is removed by the pure glass substrate (with <1% absorption of incident laser power density). What's more, the dispersed NWs will form a much thinner layer comparing with NWs from as-grown sample. Thus those two possible factors for

absorption overestimated before should be resolved much now.

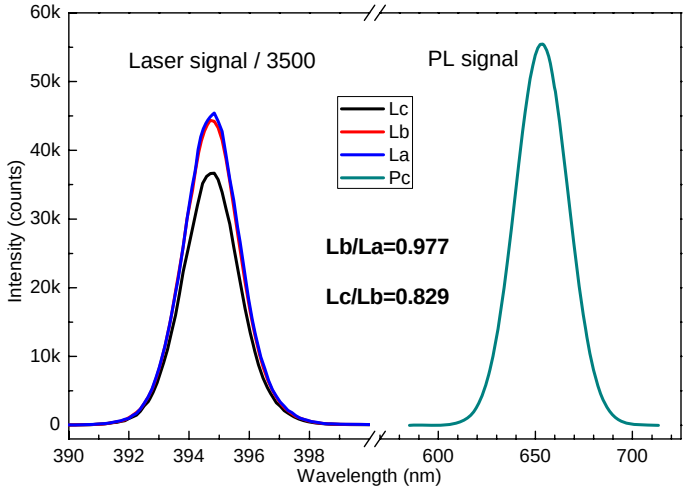

Figure 22 The PL spectra for dispersed sample

From Figure 22, we can see now the absorption from configuration B is only 2.3% (1-0.977=0.023) and 17.1% (1-0.829=0.171) from configuration C. The absorption calculated this time is more accurate compared to literature. From all dispersed samples that tested, the absorption is ranging from 7% to 35%.

Since now more accurate absorption can be achieved, we dispersed 4 spots from each as-grown sample A and B respectively and calculated their PLQE for different wavelengths. The results are plotted below.

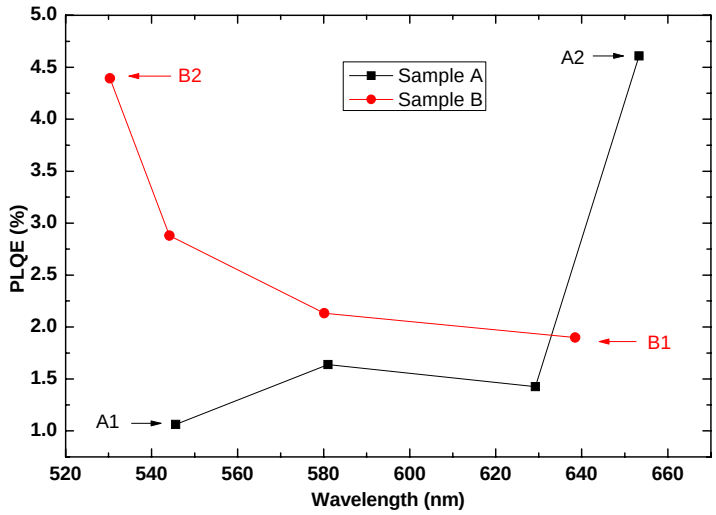

Figure 23 The PLQE result for wavelength-dependence measurement

The measured PLQE is in the range of 1.0% ~ 4.6%. It is interesting that sample A with silicon substrate have larger PLQE in CdSe rich part while sample B with quartz substrate in CdS rich part instead. This different wavelength-dependence trend I think is because the growth process is different for two samples, which leads to quality divergence of NWs. To examine this, here we define the quality factor Q for such determination, which is peak position of the PL spectrum divided by its full width at half maximum (FWHM).

$$\text{Quality Factor}\left(Q\right)=\frac{\text{peak position}\left(nm\right)}{\text{FWHM}\left(nm\right)}$$

With larger Q, the quality should be better. I have calculated the Q factor for both samples as follows:

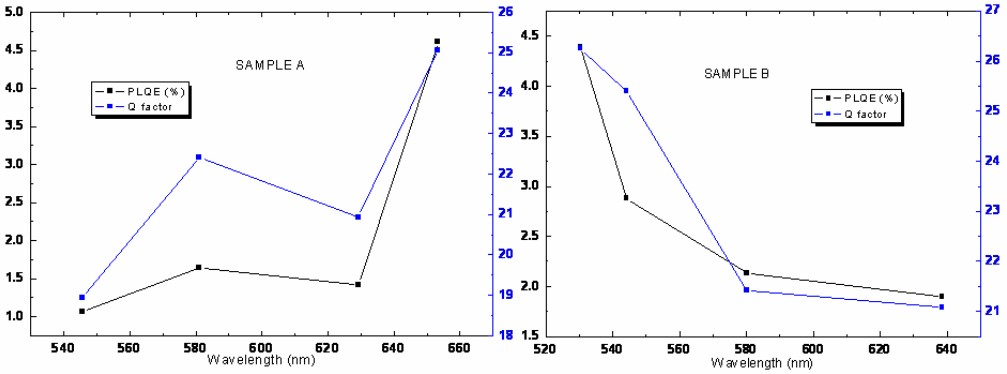

Figure 24 Comparison with Q factor and PLQE

From the figure it is easy to find the apparent relationship with PLQE and Q factor. And it meets the agreement that a larger Q factor stands for better quality from NWs. Thus at this point we can only say the PLQE has a correlation with Q factor but no apparent dependence trend with wavelength, or say, with mole fraction x.

4.5.2 Power-dependence Measurement

For deeper understanding, another set of measurements has been done by varying laser power output level with several orders of magnitude, which is known to be the power-dependence measurements. I took 4 spots from Figure 23, which noted as A1, A2 from dispersed sample A, B1, B2 from sample B respectively. The number “1” indicates the small end of PLQE while “2” the large end of it. A typical series of spectra with different level of laser output for B2 spot is shown in Figure 25 below.

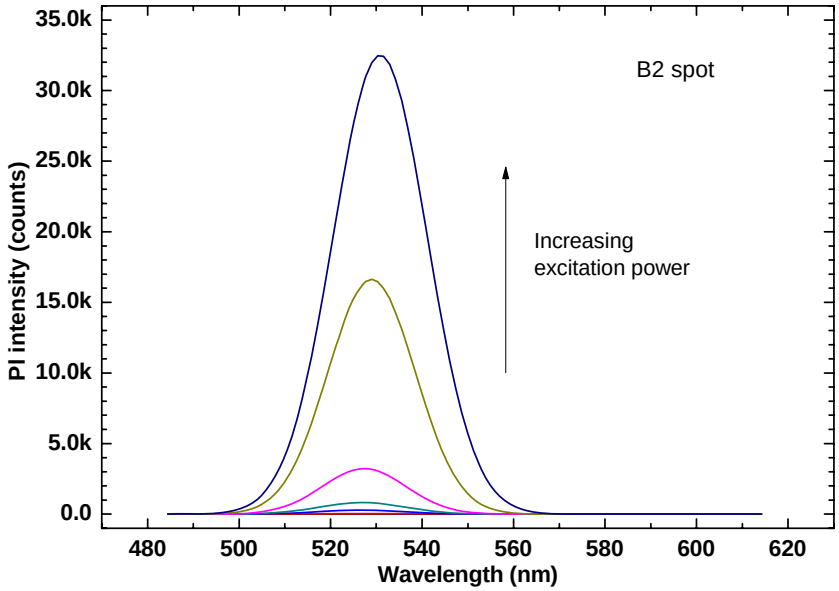

Figure 25 Power-dependence spectra on B2 spot

Based on our system, the minimum detectable laser power is about 2 orders of magnitude smaller than the original output with around 150mW (which corresponds to 4×10^8 counts after integration from our detector) at the front of sample. The PL emission intensity with power increasing in terms of counts for all 4 spots can be plotted as below in double log scale.

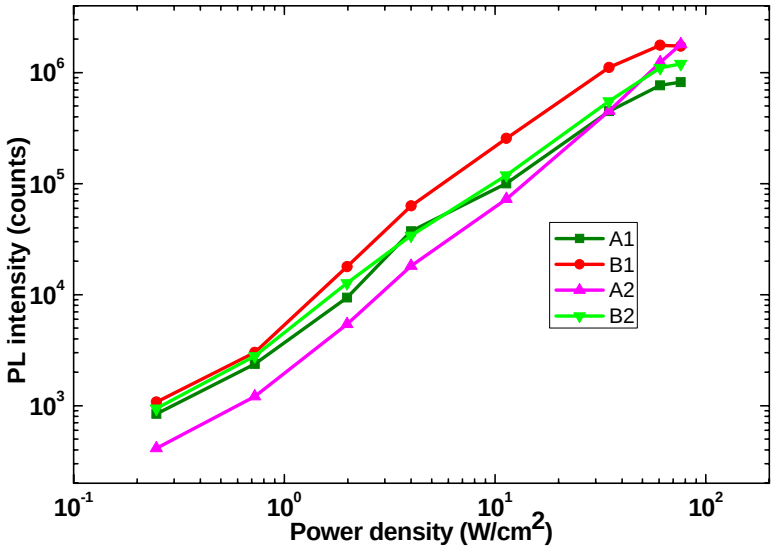

Figure 26 The relation between emission and excitation

Generally speaking, the emission intensity grows with a small super-linearity tendency as laser intensity increasing (3 orders of magnitude comparing with ~2.6 one). What's more, a strong PL emission does not necessarily mean a better PLQE since absorption is also an important factor (more important to some extent because it counts as denominator in the PLQE calculation and it is smaller than 1), take B1 as example. It indicates that PLQE measurement is more accurate and reliable for evaluate the quality of NWs comparing to PL experiments only.

For further illustration, I recorded the peak position (Figure 27) and FWHM (Figure 28) from Gaussian fitting of each spectrum of A1, B1, A2 and B2 and their relationship with laser pumping density.

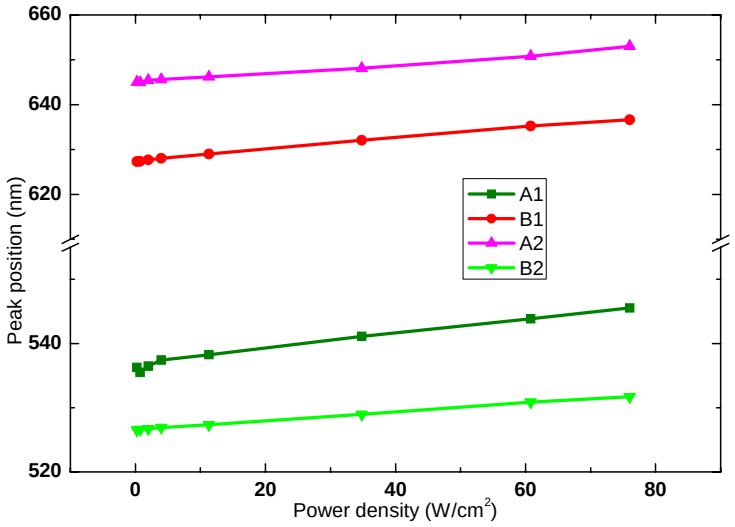

Figure 27 The relation between peak position and excitation

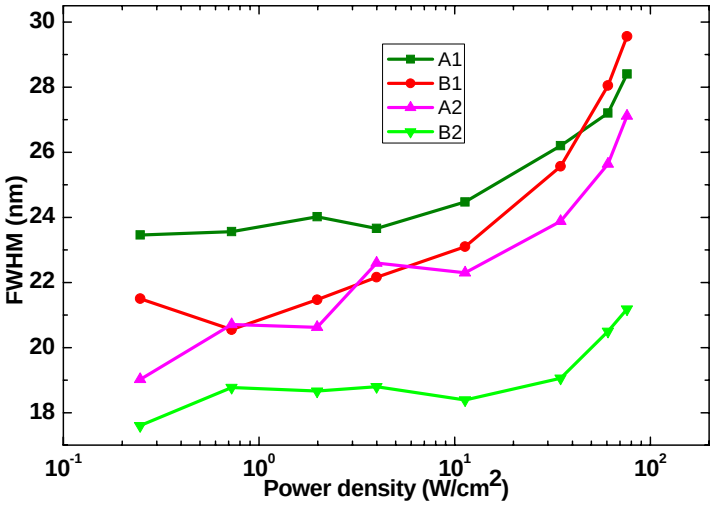

Figure 28 The relation between FWHM and excitation

From Figure 27 we can clear see 2 spots are from CdS rich side (A1 and B2) while the other 2 are from CdSe part (A2 and B1). Also we can find there exhibits red-shift of peak position (5~9 nm) as laser power density increasing. This can be explained by two possible reasons. One is due to thermal effect with increasing excitation, which will shrink the bandgap of the material to smaller

value, thus emit at longer wavelength. Another factor relates to, as mentioned before, the self-absorption of NWs. The emission is absorbed by their surrounding NWs and excites slightly longer wavelength region of the sample. It is possible since the sample itself has alloy gradient with position dependence.

For FWHM, it is apparent that all spectra are broadened with increasing laser excitation (Figure 28, 4~8 nm). This is not difficult to understand since higher excitation level will introduce more carriers and they can recombine from channels other than direct bandgap position. Also, the thermal effect will bring excess energy to carriers for realizing such process.

One thing needed to be mentioned here is that, from Figure 28, the small end of PLQE (e.g. A1 or B1 spot) represents a broader FWHM at all different excitation levels.

After investigating much on the PL emission, let's take a look at absorption now. The absorption for all 4 spots has been shown below.

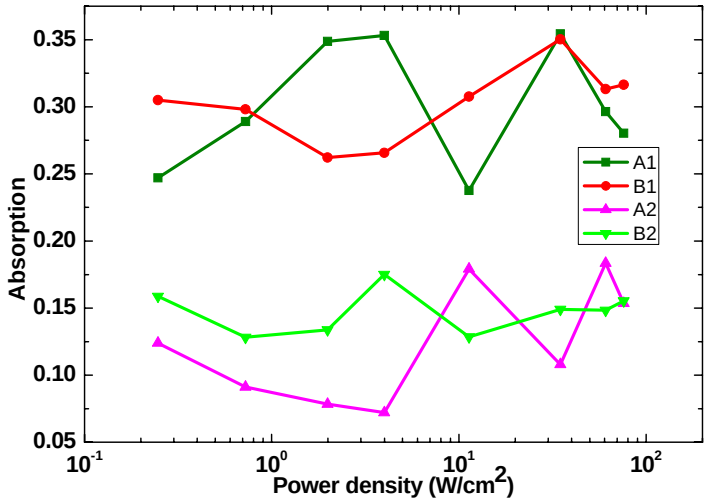

Figure 29 The relation between absorption and excitation

Generally speaking, the absorption does not vary much with increasing excitation. One may notice the spots with small absorption (i.e. A2 and B2 spots) have larger PLQE since I mentioned "2" indicates that. This also proves PLQE is a more comprehensive way for evaluating the quality of NWs since it takes the absorption into account, with the simple and convenient way for absorption measurement moreover.

With all data I got, the PLQE can be calculated and plotted in Figure 30.

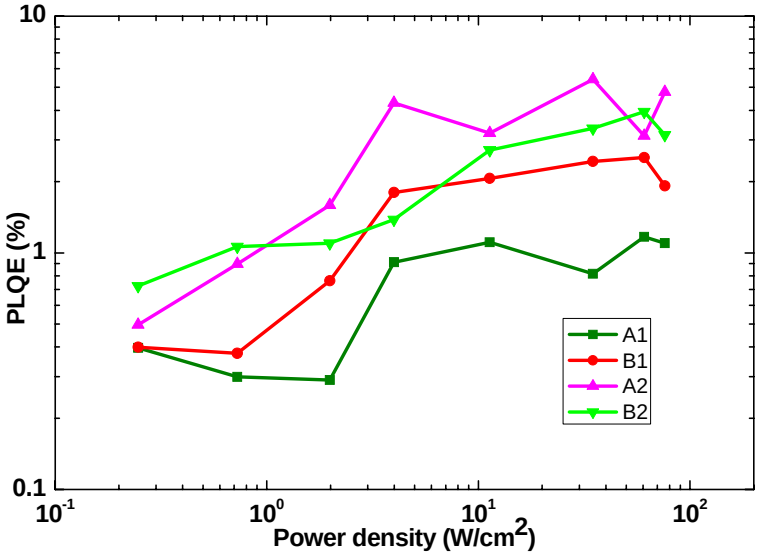

Figure 30 The PLQE result for power-dependence measurement

The PLQE is in the range of 0.3%~5.4%. We can see it is increasing with laser power density. From this trend with no apparent saturation takes place, we can anticipate the PLQE increasing more with higher excitation density. We can achieve as high as 70W/cm^2 due to system limitation. As a comparison, the group in UC Berkeley can get 2500W/cm^2 excitation with PLQE to be 20% for ZnO NWs.

Even given a larger upper limit from the system output, another factor will influence the QE value with higher excitation. A small decrease of PLQE can be observed from the highest pumping level which can be recalled from previously mentioned phenomenon about photodegradation. So next I tried to make sure if there is a direct correlation with pumping density and such phenomenon. For illustration, I chose A1 spot as an example and took the last three highest

excitations for illumination source. I recorded the peak PL emission intensity from the spectrometer for every other 5 second, as what I did for testing the photodegradation before. All intensities are taken from the same spot and the result is shown in Figure 31.

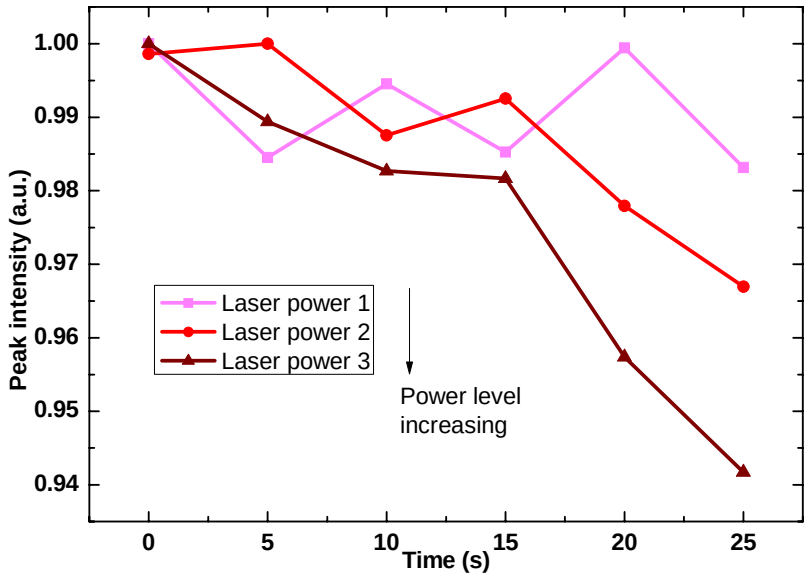

Figure 31 The relation with photodegradation and excitation intensity

For black curve, the peak intensity was oscillating within 2% range and there was no significant decrease. For red curve, which has higher excitation, the peak intensity dropped 3% from its initial value after 25 seconds irradiance. For blue curve, the even higher excitation lead to 6% decrease with same time period as red curve one. This result clearly shows that the excitation density is a responsible factor for photodegradation phenomenon. Thus there is high possibility we will encounter more severe degradation with even higher excitation then we currently have.

4.6 More about Photodegradation

It is worthy to take a bit more insight into such phenomenon. From the literature [23], it is observed in many II-VI semiconductors, such as bulk single-crystal CdS, ZnS, and ZnSe, that the luminescence intensity decreases when illuminated by ultra-violet radiation. It is believed that the rate is dependent on the power density, the exposure time, the environment, the mechanical condition of surface, and the temperature. This process is explained to be with correlation with non-equilibrium holes which localized on lattice defects in the near-surface layer.

It is further examined and shown that such degradation is dependent with surrounding environment. They used CdSe/ZnS nanocrystals with 3.2 nm diameter and with core/shell structure and illuminated with a deuterium lamp having a broad emission spectrum while maximum at 260 nm region with power density to be 0.1 mW/cm^2. The luminescence intensity decreased within the air can be shown in Figure 32.

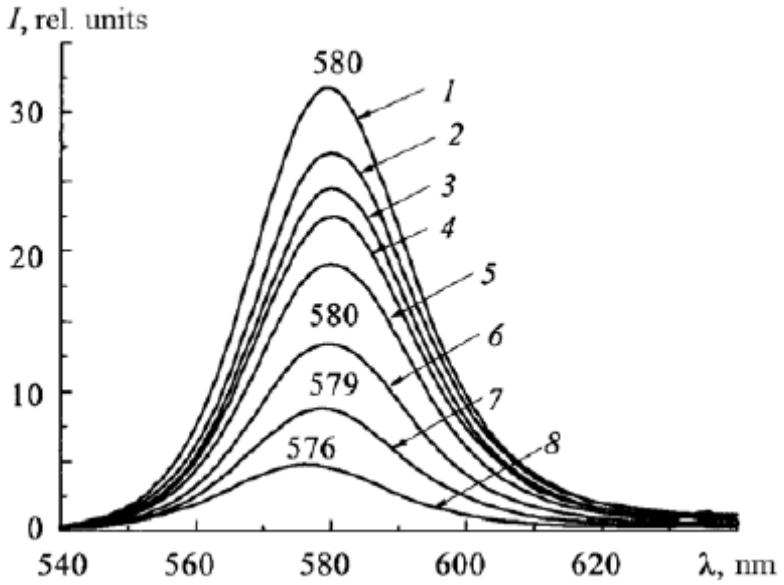

Figure 32 Photodegradation effect from literature

The numbers noted here represent increasing illumination time and corresponded to 0, 10, 20, 30, 60, 150, 300, and 600 seconds respectively. The small blue-shift here was explained to be due to the photo-oxidation process since it decreased the average size of the nanocrystals. On the other hand, within vacuum environment, where water and oxygen molecules are absence, the luminescence intensity only had a less than 10% decrease. This indicates that photo-oxidation and passivation are responsible factors for this phenomenon. However, the full understanding is still needed for more detailed mechanism, e.g. recombination process during photodegradation.

5. Summary

From PLQE measurement with integrating sphere, I found that using dispersed NWs can achieve more accurate absorption and PLQE result. Moreover, for spatial alloy gradient NWs such as $CdS_xSe_{(1-x)}$, different samples have different alloy dependence trend, which depends on growth condition. With laser pumping density increasing, the emission intensity has a positive correlation with it while there is no apparent variation of the absorption of NWs. Also, the peak position exhibits a red-shift for 5~9 nm and the spectra are broadened with 4~8 nm. During the test, I found photodegradation phenomenon with continuous laser illumination, which is proved to have relationship with pumping density. This is a limitation for using higher excitation, which may achieve larger PLQE from our experiment observation. Anyway, the measured PLQE is within the range of 0.3% ~ 5.4%, which is reasonable with comparison to literature.

References

1 Binnig, G., Rohrer, H. 1986. Scanning tunneling microscopy. *IBM Journal of Research and Development* 30 (4): 355.

2 Mårtensson, T., Patrik, C., Wacaser, B., Larsson, M., Seifert, W., Deppert, K., Gustafsson, A., Wallenberg, L., Samuelson, L. 2004. Epitaxial III-V nanowires on silicon. *Nano Letters* 4 (10): 1987-1990.

3 Björk, M.T., Ohlsson, B.J., Sass, T., Persson, A.I., Thelander, C., Magnusson, M.H., Deppert, K., Wallenberg, L.R., Samuelson, L. 2002. One-dimensional heterostructures in semiconductor nanowhiskers. Applied Physics Letters 80 (6): 1058-1060.

4 Duan, X., Huang Y., Agarwal, R., Lieber, C.M. 2003. Single-nanowire electrically driven laser. *Nature* 421: 241-245.

5 Duan, X., Huang Y., Cui. Y., Wang, J., Lieber, C.M. 2001. Indium phosphide nanowires as building blocks for nanoscale electronic and optoelectronic devices. *Nature* 409: 66-69.

6 Liu, Y.H., Wayman, V.L., Gibbons, P.C., Loomis, R.A., Buhro, W.E. 2010. Origin of high photoluminescence efficiency in CdSe quantum belts. *Nano Letters* 10 (1): 352-357.

7 Huang, Y., Duan, X., Cui, Y., Lauhon, L., Kim, K., Lieber, C.M. 2001. Logic gates and computation from assembled nanowire building blocks. *Science* 294: 1313-1317.

8 Yu, Y., Protasenko, V., Jena, D., Xing, H., Kuno, M. 2008. Photocurrent polarization anisotropy of randomly oriented nanowire networks. *Nano Letters* 8: 1352.

9 Barrelet, C.J., Greytak, A.B., Lieber, C.M. 2004. Nanowire photonic circuit elements. *Nano Letters* 4: 1981-1985.

10 Cui, Y., Wei, Q.Q., Park, H.K., Lieber, C.M. 2001. Nanowire nanosensors for highly sensitive and selective detection of biological and chemical species. *Science* 293 (5533): 1289-1292.

11 Pankove, J.I. 1971. *Optical process in semiconductors.* New York: Dover Publications.

12 Yu, P.Y., Cardona, M. 2004. *Fundamentals of semiconductors: Physics and materials properties.* Berlin: Springer.

13 Scholes, G.D., Rumbles, G. 2006. Exciton in nanoscale systems. *Nature materials* 5: 683-696.

14 Matioli, E., Weisbuch, C. 2010. Direct measurement of internal quantum

efficiency in light emitting diodes under electrical injection. *Journal of Applied Physics* 107: 053114.

15 Mello, J.C., Wittmann, H.F., Friend, R.H. 1997. An improved experimental determination of external photoluminescence quantum efficiency. *Advanced Materials* 9 (3): 230-232.

16 Technical guide: integrating sphere theory and applications. Labsphere®

17 Georgiev, G.T., Butler, J.J. 2007. Long-term calibration monitoring of Spectralon diffusers BRDF in the air-ultraviolet. *Applied Optics* 46 (32): 7892-7899.

18 Pan, A.L., Zhou, W.C., Leong, E.S.P., Liu, R.B., Chin, A.H., Zou, B.S., Ning, C.Z. 2009. Continuous alloy-composition spatial grading and superbroad wavelength-tunable nanowire lasers on a single chip. *Nano Letters* 9 (2): 784-788.

19 Pan, A.L., Liu, R.B., Sun, M.H., Ning, C.Z. 2010. Spatial composition grading of quaternary ZnCdSSe alloy nanowires with tunable light emission between 350 and 710 nm on a single substrate. ACS Nano 4 (2): 671-680.

20 Klyachkovskaya, E.V., Vashchenko, S.V., Stupak, A.P., Gaponenko, S.V. 2010. Photodegradation of CdSe/ZnS semiconductor nanocrystals in a polymer film in air and under vacuum. *Journal of Applied Spectroscopy* 77 (5): 732-736

21 Vietmeyer, F., Frantsuzov, P.A., Janko, B., Kuno, M. 2011. Carrier recombination dynamics in individual CdSe nanowires. *Physics Review B* 83: 115319.

22 Gargas, D.J., Gao, H.W., Wang. H., Yang, P.D. 2011. High quantum efficiency of band-edge emission from ZnO nanowires. *Nano Letters* 11: 3792-3796.

23 Yablonskii, G.P., Belyaeva, A.K., *Fizika i Khimiya Obrabotki Materialov* 4: 30-34.